Desalination and Water Treatment
www.deswater.com

doi: 10.5004/dwt.2020.25646

190 (2020) 156–166
June

Silica-functionalized graphene oxide/ZnO as a photocatalyst for degradation of pirimiphos-methyl from aqueous solutions

Hossein Arfaeinia[a,b], Ramin Khaghani[a,*], Mehdi Fazlzadeh[c], Yousef Poureshgh[c]

[a]*Department of Medical Parasitology, School of Medicine, Aja University of Medical Sciences, Tehran, Iran, Tel. +989128162383; email: khagha_r@yahoo.com (R. Khaghani), Tel. +989178844836; email: Arfaeiniah@yahoo.com (H. Arfaeinia)*
[b]*Department of Environmental Health Engineering, School of Health and Nutrition, Bushehr University of Medical Sciences, Bushehr, Iran*
[c]*Social Determinants of Health Research Center, Ardabil University of Medical Sciences, Ardabil, Iran, Tel. +989148092356; email: yusef.poureshg@gmail.com (Y. Poureshg), Tel. +989127035079; email: m.fazlzadeh@gmail.com (M. Fazlzadeh)*
[d]*Department of Environmental Health Engineering, School of Health, Tehran University of Medical Sciences, Tehran, Iran*
[e]*Department of Environmental Health Engineering, School of Health, Ardabil University of Medical Sciences, Ardabil, Iran*

Received 21 August 2019; Accepted 9 February 2020

ABSTRACT

Photocatalytic degradation of pirimiphos-methyl using silica-functionalized graphene oxide (GO)/ZnO incorporated with fiberglass (silica-GO/ZnO) was evaluated. The effect of different variables including the initial concentration of pirimiphos-methyl, temperature, contact time, and hydrogen peroxide concentration was tested on the photocatalytic degradation. Moreover, the effect of co-existing organic compounds (folic acid, citric acid, oxalate, phenol, and ethylenediaminetetraacetic acid) and different purging gases (oxygen and nitrogen) was explored. The maximum removal efficiency was achieved at a neutral medium, in other words at acidic and alkaline conditions the catalyst corrosion occurred which resulted in a decrease in efficiency. By increasing the temperature, the photocatalytic removal efficiency using silica-GO/ZnO increased, because of the catalyst expansion and therefore, greater availability of functional groups. With an increase in the concentration of pollutant from 5 to 60 mg/L, the k_{obs} values decreased from 0.050 to 0.005, while the electrical energy per order (E_{E0}) increased from 95.81 to 923.12 kWh/m^3. The removal efficiency of pirimiphos-methyl in the absence of hydrogen peroxide under the optimal conditions of other factors was obtained by ≈98%. However, as the concentration of hydrogen peroxide increased from 3 to 45 mM, the removal efficiency decreased from 86.74% to 81.61%, respectively. The presence of organic compounds acted as a scavenger and resulted in reduced removal efficiency. The findings of this study also suggested that purging of oxygen gas provided greater photocatalytic activity compared to nitrogen and ambient air for the degradation of the target contaminant.

Keywords: Photocatalyst; ZnO; Pirimiphos-methyl; Aqueous solutions

1. Introduction

Today, the consumption of large amounts of pesticides in agriculture, different industries, and others have resulted in the contamination of different environmental matrices. Organophosphorus (OP) pesticides are one of the most important groups of chemicals which are extensively used worldwide to control pests [1,2]. Since these chemicals are detected in water resources, therefore monitoring OP pesticides has been incorporated in many plans of supervising contamination of groundwater across different countries [3,4]. This further reflects that these pollutants have a high

* Corresponding author.

capacity for leaching to groundwater and contaminating hydrologic systems [5,6]. The use of pesticides in agricultural areas and the transport of pesticides by container and spray equipment may cause contamination of water resources in the high concentration range (1–50 μ/L) [7]. Thus, the protection of water resources requires novel technologies for the oxidation of pesticides from agricultural drains before entering to water bodies.

Many techniques such as adsorption [8], reduction with nanoscale zerovalent iron particles [9], biological methods [10], ozonation technology [11], photolysis [12], Fenton, and photo-Fenton processes [13] have been applied to remove pesticides from aqueous solutions. However, these techniques have some restrictions such as cost-ineffectiveness and operational difficulty [14–17]. For instance, adsorption just separates contaminants from water to a solid phase without any degradation [18–20]. The biological method generally requires long times for treatment [21,22]. Photocatalytic systems are the most effective and economical approach which do not have the above-mentioned limitations and can be used for treating a wide range of concentrations [23–26]. In this regard, zinc oxide (ZnO) has been used in many researches as a photocatalyst for the treatment of organic pollutants due to its good properties like suitable photosensitivity and energy band [27,28]. Nevertheless, the direct usage of zinc oxide has some challenges including fast recombination of the photo-generated electron-hole pairs and limited photo-responding range [29] that have led to its performance decline. Therefore, in order to enhance its photocatalytic performance, a series of solutions has been proposed including structural design [30], noble metal loading [31], ion doping [32], and coupling with another semiconductor [33]. It has been suggested that these factors cause enhanced photocatalytic efficiency of ZnO through increasing the range of photo-sorption and preventing electron-hole recombination [34]. Another solution to overcome these limitations is the use of materials with carbon structure like graphene [35]. Graphene is a carbon material which acts as a good electron transmitter and receptor material, accelerating the transmission of photon-derived electrons. Further, due to electron interactions with semiconductors, it prevents the recombination of electric charge in electron transfer processes, thereby enhancing the photocatalytic performance [36]. In addition, the properties of high surface area and high adsorption capacity of graphene lead to increased contact between the pollutant and the photocatalyst agent [37]. These factors improve the efficiency of target pollutant removal. Meanwhile, graphene oxide (GO) has attracted a great deal of attention due to possessing similar features to graphene as well as a specific superficial structure containing carboxyl and hydroxyl functional groups [38]. In particular, combining GO with semiconductors offers several positive results including high adsorption of pollutants, wide range of photo-sorption, separation, and effective charge transfer [37,39]. Therefore, it is believed that if ZnO nanostructures are properly coated on GO sheets, it is possible to achieve a good photocatalytic performance.

Selection of suitable support is very essential for heterogeneous liquid–solid photocatalytic processes. Thus, the catalyst like powdered GO/ZnO composite should be fixated on a solid-state material before contacting pollutant molecules. Fiberglass is a solid-state material that has been widely used over the last decade for fixation of nanomaterials owing to low cost, lightweight, easy attachment, suitable transparency for natural light, and great stability against ultraviolet radiation as well as excellent mechanical properties [40,41]. In our previous study, the silica-GO/ZnO was successfully utilized for photocatalytic removal of benzene from a polluted airflow [42].

Nevertheless, the photocatalytic characteristics in the liquid medium and the efficiency of the contaminant treatment using silica-GO/ZnO composite are still unclear. Thus, in the current study, for the first time, silica-GO/ZnO was tested for photocatalytic removal of pirimiphos-methyl (an organophosphorus pesticide) from aqueous solutions. Pirimiphos-methyl has a high potential for oxidation and stable chemical structure which makes it a suitable option for assessing photocatalytic properties of silica-GO/ZnO incorporated fiberglass composite.

2. Materials and methods

2.1. Photocatalytic setup

A Pyrex photoreactor equipped with ultraviolet 125 W medium pressure UVC-lamp was used for the removal of pirimiphos-methyl from aqueous solutions. The utilized reactor consisted of two parts. The outer part had 2 L-solution capacity and the internal section contained the UV lamp. The UVC lamp used in this study was a medium pressure with a maximum wavelength of 247.3 nm and a photo intensity of 1,020 mcW/cm^2. In addition to the two sections above, a section outside the reactor with a capacity of 12 L was designed to keep the reactor temperature (25°C) constant throughout the experiments. The photocatalytic reactor operated in a batch mode. The preparation method and properties of the silica-GO/ZnO catalyst were fully described in our previous study [42]. The pH_{zpc} parameter of the synthesized catalyst was measured by pH drift method [43]. The catalyst coated on the vertical wall and bottom of the reactor using fiberglass glue. The coated wall was 6 cm away from the UV lamp. All of the photocatalytic experiments were performed in 100 mL of the aqueous solution. Fig. 1 shows a schematic diagram of the experimental reactor.

2.2. Process of experiments and analysis

The effect of different variables including the initial concentration of pirimiphos-methyl, pH, temperature, contact time, and hydrogen peroxide concentration was evaluated. This study also evaluated the effect of co-existing organic compounds (folic acid, citric acid, oxalate, phenol, and ethylenediaminetetraacetic acid) and different purging gases (oxygen and nitrogen). The stock solution (1,000 mg/L) of pirimiphos-methyl was prepared through dissolving pirimiphos-methyl in distilled water and the intended concentrations were prepared by dilution of the stock solution. The initial pH of the solution was adjusted by adding 0.1 N HCl and 0.1 N NaOH, which was then measured by a pH meter (Metron, Switzerland). All of the experiments were performed at 25°C ± 1°C in the laboratory. To perform the photocatalytic removal process, a

solution containing pirimiphos-methyl was prepared and poured into the reactor. It was then left for 30 min to reach equilibrium (under the dark condition). Subsequently, the radiation source was turned on and the photocatalytic process was performed under the determined conditions. Following the process, the sample was withdrawn from the supernatant and passed through Whatman filter paper 16 in order to remove the possible catalyst particles. To determine the residual pirimiphos-methyl concentration, the high-performance liquid chromatography (HPLC, Waters, USA) device was used. The detector utilized in this device was a UV-visible detector (4900 CE) and the selected wavelength was 245 nm. Further, 20 μL-sample was injected into a c18 analytic column, and the mobile phase was pumped into the column with a flow rate of 0.9 mL/min. For determining the byproducts resulting from the degradation of pirimiphos-methyl through the process, the gas chromatography-mass spectrometry device (Varian-GC–MS 4000) was utilized. The column in this device was HP-522 and its carrier gas was helium with a flow rate of 1 mL/min. Moreover, kinetic evaluations were carried out and simulated with zero-, first- and second-order, and Langmuir Hinshelwood kinetic model. The electrical energy per order (E_{E0}) was also calculated to assess the cost-efficiency of the degradation processes. The kinetics equations, parameters, and constants are given in Table 1.

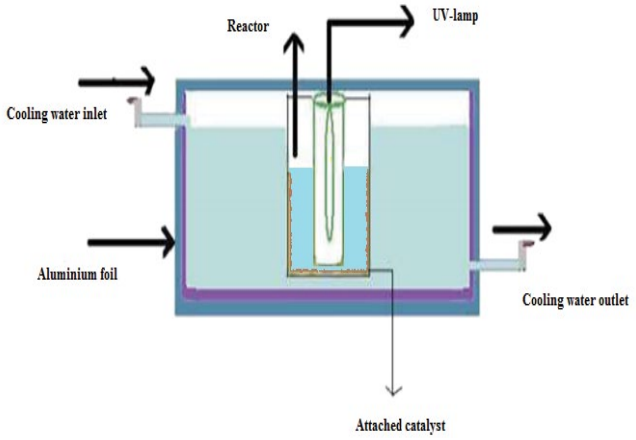

Fig. 1. Schematic diagram of the experimental reactor.

3. Results and discussion

3.1. Catalyst characteristics

N_2 adsorption–desorption isotherm (at 77 K) was carried out to investigate the surface area and volume of the pores in GO/ZnO and silica-GO/ZnO catalysts (Fig. 2). The isotherms mostly were in the form of IV-type isotherms, implying that the synthesized catalyst is porous. In Fig. 2, it can be observed that silica-GO/ZnO has a greater porosity compared to GO/ZnO particles. In addition, the total pore volume in silica-GO/ZnO composite (0.14 cm^3/g) is larger than that of GO/ZnO (0.06 cm^3/g). The large pore volume in silica-GO/ZnO can be attributed to the formation of secondary pores which originates from close stack among the GO/ZnO particles. The Brunauer–Emmett–Teller surface area for silica-GO/ZnO and GO/ZnO was calculated as 23.90 and 30.20 m^2/g, respectively. This suggests that the addition of silica to GO/ZnO could enhance the specific area, which in turn improves the adsorption capacity. Therefore, it can be a suitable option as a kind of adsorption substance.

The crystalline structure of the catalyst was determined by X-ray diffraction (XRD) analysis, as shown in Fig. 3. As can be seen in the figure, a common peak exists at 2θ = 12 in both graphs of GO (b) and Si/GO (c), which is related to GO and is consistent with previous studies [44,45]. A considerably wide peak is also observed at 2θ = 20–30 from Si-GO graph (c), which represents halo of amorphous silica. This suggests that SiO_2 nanoparticles have been successfully coated on the surface of graphene oxide nanoplates. According to Bragg's law, ($n\lambda = 2d \sin\theta$, $\lambda = 0.154$ nm), *d*-spacing for Si-GO was calculated as 7.33 Å, which had diminished compared with 8.12 Å for GO. The reason for this issue is the decoration of silica on graphene [46]. In ZnO graph (d), again the peaks at 2θ = 32, 34, and 36 are related to planes 100, 102, and 101 of hexagonal wurtzite ZnO, respectively. In Si-GO/ZnO graph (e), in addition to the peaks at 2θ = 12 and 2θ = 20–30, which are related to GO and SiO_2, respectively, a good crystalline structure of zinc oxide nanoparticles is observed even after the immobilization. The mean crystalline size of zinc oxide nanoparticles was calculated by Debye–Sherrer equation. Based on this equation, the mean crystalline size of zinc oxide and zinc oxide coated on the composite was calculated as 56.6 and 54.1 nm, respectively. The results suggest a minor effect of immobilization on the size of pure zinc oxide nanoparticles.

Table 1
Kinetic models and their parameters

Kinetic models	Electrical energy per order	Parameters
Zero-order: $C_0 - C_t = k_0 t$		
First-order: $\ln\frac{C_0}{C_t} = k_{obs} t$	$E_{E0} = \frac{38.4 \times P}{V \times k_{obs}}$	C_0 (mg/L), C_t (mg/L), k_0 (mol/L min), k_{obs} (1/min), k_2 (mol/L min), $[\text{pirimiphos-methyl}]_0$ (mg/L), k_c (mg/L min), $k_{\text{pirimiphos-methyl}}$ (L/mg), P (kW), V (L), E_{E0} (kWh/m^3)
Second-order: $\frac{1}{C_0} - \frac{1}{C_t} = k_2 t$	$E_{E0} = \frac{P \times t \times 1{,}000}{V \times 60 \times \log\left(\frac{C_i}{C_f}\right)}$	

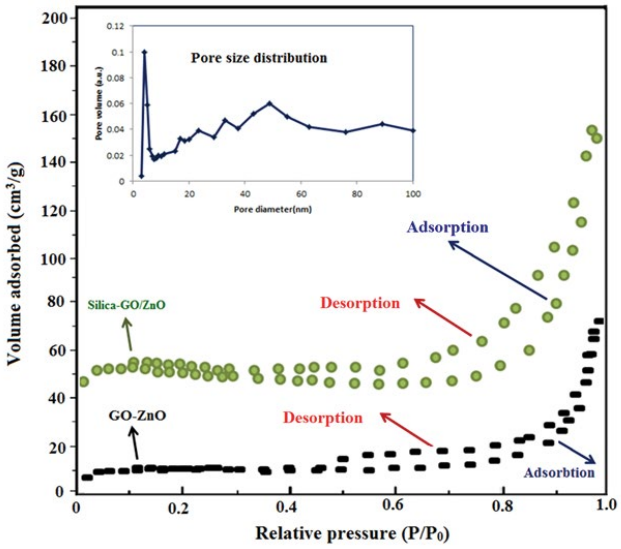

Fig. 2. Nitrogen adsorption–desorption isotherms at 77 K for GO-ZnO and Si-GO/ZnO composites and pore size distributions for silica-GO-ZnO composite.

Other characteristics of the synthesized catalyst are given in our previous research [42].

3.2. Effect of initial pH on the photocatalytic removal of pirimiphos-methyl

The effect of initial pH on the photocatalytic removal of pirimiphos-methyl through the silica-GO/ZnO incorporated fiberglass composite was investigated. For this purpose, the concentration of pirimiphos-methyl (30 mg/L) and temperature (25°C) were considered constant, while pH values were altered between 3 and 10. Then, the extent of removal of the pollutant was measured for the studied pHs. The results provided in Fig. 4. As can be seen, with the elevation of the initial pH from 3 to 7, the removal efficiency increased from around 59%–98%. However, with the further rise of pH from 7 to 10, the efficiency diminished and reached to around 30%. Generally, considerable changes were observed in the removal efficiency of the pollutant with pH variations. The major reason for the high degradation of this pollutant at acidic pH can be photo-corrosion of ZnO particles under acidic and alkaline conditions [47]. The pH_{zpc} factor of the silica-GO/ZnO catalyst was obtained around 8.13. According to previous studies, pH_{zpc} of ZnO nanoparticles is around 9 [47]. The pK_a value for the pirimiphos-methyl is 4.3 [48]. The different photocatalytic activity observed at different pHs can be explained by different electrostatic interactions between the ZnO surface and pirimiphos-methyl [49]. Since pK_a value for pirimiphos-methyl is 4.3, at pH above 4.3, it has a negative charge, while the silica-GO/ZnO photocatalyst at pHs below 8.13 has a positive charge. Therefore, the maximum removal of pirimiphos-methyl occurs when pH was between $pK_a^{pirimiphos\text{-}methyl}$ and $pH^{silica\text{-}GO/ZnO}$. In these conditions, negative charge primiphos-methyl is easily attached by the positively charged silica-GO/ZnO catalyst [50]. At high pHs, both the silica-GO/ZnO catalyst and pirimiphos-methyl have a negative charge, and thus the electrostatic repulsion between them leads to diminished absorption of the molecules of this pollutant on the catalyst surface, thereby reducing the removal efficiency [49,51]. Tabasideh et al. [52] have attained the maximum degradation percentages for diazinon at pH 6.5 and the degradation rate was decreased at the alkaline media. The photocatalytic degradation of diazinon increased with increasing pH up to 5.2 and then decreased [47]. In this study, the solution pH of 7 was obtained as the optimal pH for removal of pirimiphos-methyl, and the rest of the experiments were performed at this pH.

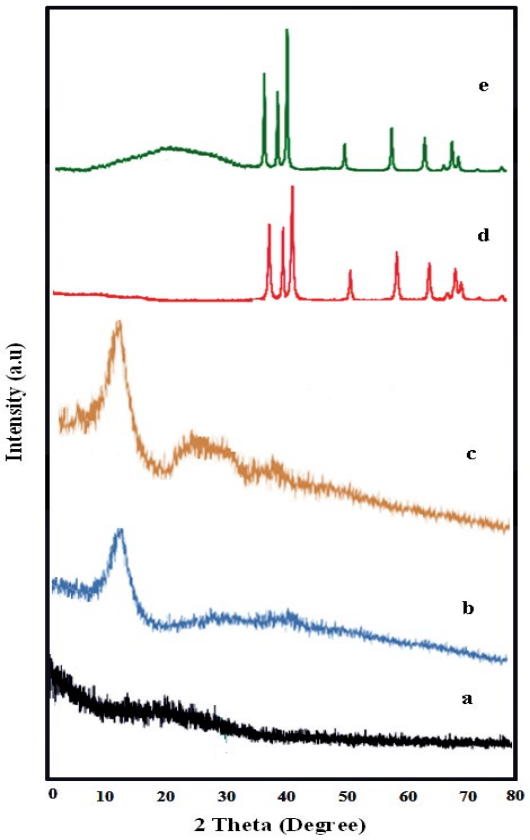

Fig. 3. Typical XRD patterns of samples: (a) fiberglass, (b) GO, (c) Si-GO, (d) ZnO, and (e) FG/GO-SiO_2-ZnO.

3.3. Effect of initial concentration on the photocatalytic removal of pirimiphos-methyl

The removal of pirimiphos-methyl was investigated across five different concentrations (5, 15, 30, 45, and 60 mg/L), pH = 7, and 25°C (Fig. 5). As can be seen, the removal efficiency of the pollutant found a descending trend with an elevation of its initial concentration. With the rise in the initial concentration from 5 to 60 mg/L, over 100 min of contact time, the photocatalytic removal of pirimiphos-methyl decreased from around 100% to 39%. The main reason for this reduction with concentration rise is the increased ratio of the number of molecules of pirimiphos-methyl to the number of active sites available across the silica-GO/ZnO catalyst surface. In other words, the high content of the pollutant exerts an inhibitive effect on the reaction between the pollutant

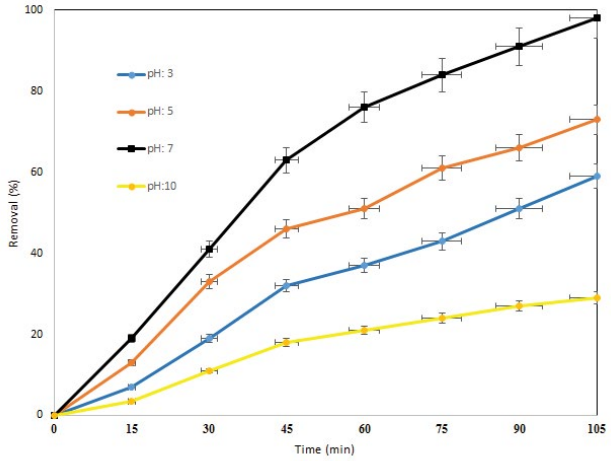

Fig. 4. Influence of initial pH on the photocatalytic degradation of pirimiphos-methyl through silica-functionalized graphene oxide/ZnO.

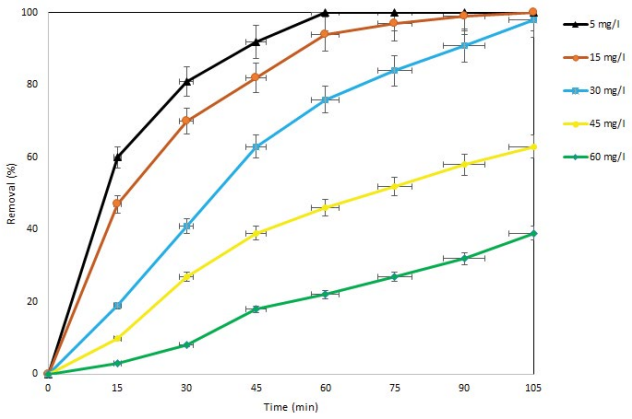

Fig. 5. Influence of initial concentrations on the photocatalytic degradation of pirimiphos-methyl through silica-functionalized graphene oxide/ZnO.

molecules and photogenerated holes or hydroxyl radicals. Therefore, due to the absence of any direct contact between them, the removal efficiency drops [53,54]. The statistical test also confirmed that the pirimiphos-methyl removal efficiency is significantly affected by its initial concentration in the interval contact time of reaction (p-value < 0.05). On the other hand, based on F-value, the initial concentration has been the most influential factor affecting the removal efficiency of the pollutant (F-value = 241.56). Similar results have been reported by other researchers [50,55]. In previous studies, it was reported that applying a higher concentration of nanoparticles would reduce light penetration into the medium, which brings about decreasing photodegradation efficiency [52,56,57].

3.4. Effect of temperature on the photocatalytic removal of pirimiphos-methyl

This study also examined the effect of reaction temperature on the photocatalytic removal of pirimiphos-methyl by the silica-GO/ZnO incorporated fiberglass. For this purpose, the concentration of pirimiphos-methyl and pH were considered as 30 mg/L and 7, respectively, while different values of temperature (20°C, 25°C, 35°C, 45°C, and 50°C) were applied. The results displayed in Fig. 6. As can be observed, the photocatalytic removal efficiency of pirimiphos-methyl has increased with increasing the reaction temperature. With temperature elevation from 20°C to 50°C, the removal efficiency has grown from 89% to 100%. The reason for this efficiency augmentation is that temperature is one of the influential and important factors in $OH^{\bullet}$-based-AOPs. Hence, with temperature elevation, the extent of production of hydroxyl radicals increases, causing enhanced efficiency of the process [58]. Also, this efficiency growth can be attributed to the fact that higher temperatures cause expansion of the silica-GO/ZnO catalyst. As a result, the functional groups present on its surface become more available in the solution, thereby enhancing the removal efficiency [59]. In other words, the increase in removal with the rise of temperature may be due to the accessibility of oxidative species originating from active sites at the catalyst surface [60]. Moreover, higher reaction temperatures produce more cavitation bubbles for degrading organic pollutants [61].

3.5. Kinetics of the photocatalytic degradation of pirimiphos-methyl and electrical energy per order

The laboratory findings resulting from catalytic degradation of pirimiphos-methyl at different reaction times were applied with zero-, first-, and second-order kinetic models. Also, the relationship between the primary photocatalytic degradation rate and the initial concentration of pirimiphos-methyl was represented by the Hinshelwood–Langmuir model. In this study, this factor (E_{E0}) was evaluated. The E_{E0} value for the photocatalytic degradation of pirimiphos-methyl is defined as the number of kWh of electric energy that is required for the concentration of the pollutant to be removed by one order of magnitude (equivalent to 90%) in 1 m^3 of contaminated water.

In order to achieve the kinetic parameters of pirimiphos-methyl degradation, C_0–C_t, $\ln[C_0/C_t]$, and $[1/C_0–1/C_t]$ terms were drawn vs. time (t). The kinetic parameters as well as the zero-, first-, and second-order reactions for the photocatalytic degradation of pirimiphos-methyl across different concentrations and initial pHs are presented in Tables 2 and 3, respectively. Based on the findings, it can be observed that the photocatalytic degradation of pirimiphos-methyl follows the first-order kinetic model. As can be seen in Table 2, with the elevation of the initial concentration of pirimiphos-methyl from 5 to 60 mg/L, the reaction rate of the first-order kinetic model (k_{obs}) and R^2 have decreased from 0.0501 to 0.0051 and from 0.9963 to 0.8919, respectively. In order to obtain the k_{obs} values at different initial concentrations, first $\ln[\text{pirimiphos-methyl}_0/\text{pirimiphos-methyl}]$ was drawn against the reaction time, and the resulting slope line was considered as k_{obs}. The $K_{\text{pirimiphos-methyl}}$ and k_c values were also obtained as 0.181 and 0.219 mg/L min by drawing the $1/k_{obs}$ against the initial concentration of pirimiphos-methyl.

E_{E0} values for the studied processes are also provided in Table 2. As can be seen, with the elevation of the initial concentration from 5 to 60 mg/L, the E_{E0} value increased

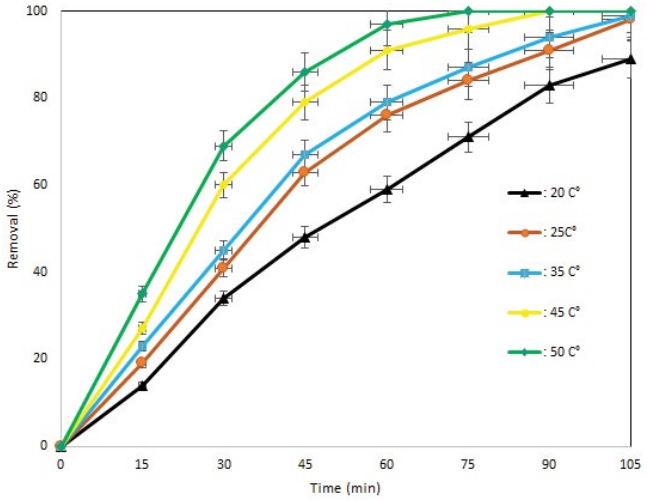

Fig. 6. Influence of temperature on the photocatalytic degradation of pirimiphos-methyl through silica-functionalized graphene oxide/ZnO.

from 95.81 to 923.12 kWh/m^3. The E_{E0} value required for the UV/silica-GO/ZnO process (163 kWh/m^3) has been less than that of UV/ZnO (655 kWh/m^3), UV/GO (897 kWh/m^3), and UV (1,153 kWh/m^3).

3.6. Effect of adding H_2O_2 and organic scavengers

In order to determine the effect of hydrogen peroxide and organic scavengers, a series of experimental runs were performed within the concentration range of 3–45 mM and at a constant concentration of 25 mg/L of organic compounds (citric acid, folic acid, oxalate, EDTA, humic acid, and phenol). The initial concentration of the pollutant, temperature, and pH were kept constant at 30 mg/L, 25°C, and 7, respectively. The results of the effect of adding H_2O_2 are visualized in Fig. 7. As can be seen in Fig. 7, the extent of removal of pirimiphos-methyl has diminished with the elevation of the hydrogen peroxide concentration. More specifically, the removal efficiency in the absence of this oxidant has been around 98%. However, with the elevation of the hydrogen peroxide concentration from 3 to 45 mM, the removal efficiency of this pollutant dropped from 86.74% to 81.61%, respectively. This reduction in the removal efficiency can be attributed to the fact that hydrogen peroxide, according to the following equations, can act as a powerful radical scavenger, and thus through reducing the hydroxyl radicals causes diminished degradation of this pollutant [62]. According to statistical tests, the removal efficiency of pirimiphos-methyl toxin has been significantly affected by altering the concentration of hydrogen peroxide from 3 to 45 mmol (p-value < 0.05).

$$HO_2^{\bullet} + HO^{\bullet} \rightarrow H_2O + O_2 \quad (1)$$

$$H_2O_2 + h_{VB}^{"} \rightarrow H^+ + HO_2^{\bullet} \quad (2)$$

The effect of the addition of organic compounds (citric acid, folic acid, oxalate, EDTA, humic acid, and phenol) is also depicted in Fig. 8. As can be observed, the photocatalytic degradation efficiency of pirimiphos-methyl has been negatively affected by addition of these organic compounds [without adding scavengers (98%), humic acid (47.83%), folic acid (84.54%), citric acid (60.12%), EDTA (81.93%), oxalate (79.44%), and phenol (65.43%)]. These observations can be attributed to the fact that this group of organic compounds also act as radical scavengers [63], and reduce the number of hydroxyl radicals available for degradation of pollutants [54].

3.7. Effect of purging gases

To determine the effect of purging gases, a series of experiments were performed with the purging of nitrogen and oxygen at the low rate of 2.5 L/min, pirimiphos-methyl concentration of 30 mg/L, the temperature of 25°C, and pH 7. The results are presented in Fig. 9. As can be seen, the purging of oxygen gas provided greater photocatalytic activity compared to nitrogen and ambient air for the degradation of the contaminant. Upon addition of oxygen, the removal efficiency of the pollutant increased from 31% to 100% during 5–100 min, while this range with the ambient air and in the presence of nitrogen increased from 19% to 98% and from 14% to 73%, respectively. In this series of experiments, the extent of dissolved oxygen over the course of the reaction was also measured (Fig. 9). As can be seen, the extent of dissolved oxygen diminished with prolongation of contact from 10 to 100 min, falling from 20.12 to 12.17 mg/L. These findings suggest the significant role of the dissolved oxygen in photocatalytic reactions. Dissolved oxygen through reaction with

Table 2
Kinetic models for the degradation of pirimiphos-methyl via UV/silica-GO/ZnO at different initial concentrations (temperature = 25°C and pH = 7)

[Pirimiphos-methyl]$_0$, mg/L	Zero-order			First-order			Second-order	
	k_0 (mol/L min)	R^2	k_{obs} (1/min)	1/k_{obs} (min)	R^2	E_{E0} (kWh/m^3)	k_2 (mol/L min)	R^2
5	0.0631	0.5767	0.0501	20.011	0.9963	95.81	0.4711	0.7443
15	0.1241	0.6334	0.0161	64.081	0.9732	306.21	0.0129	0.8976
30	0.1399	0.7992	0.0101	105.991	0.9391	509.33	0.0008	0.9906
45	0.1539	0.8483	0.0060	179.021	0.9217	857.12	0.0003	0.9454
60	0.1899	0.8323	0.0051	192.016	0.8919	923.12	0.0001	0.9111

Table 3
Kinetic models for the degradation of pirimiphos-methyl via UV/silica-GO/ZnO at different initial pHs (temperature = 25°C and [pirimiphos-methyl]$_0$ = 30 mg/L)

pH	Zero-order		First-order		Second-order	
	k_0 (mol/L min)	R^2	k_1 (1/min)	R^2	k_2 (mol/L min)	R^2
3	0.0931	0.8439	0.0084	0.9512		0.9912
5	0.1019	0.7731	0.0117	0.9271		0.9876
7	0.1251	0.6567	0.0311	0.9656		0.9123
10	0.0599	0.9761	0.0052	0.9878		0.9949

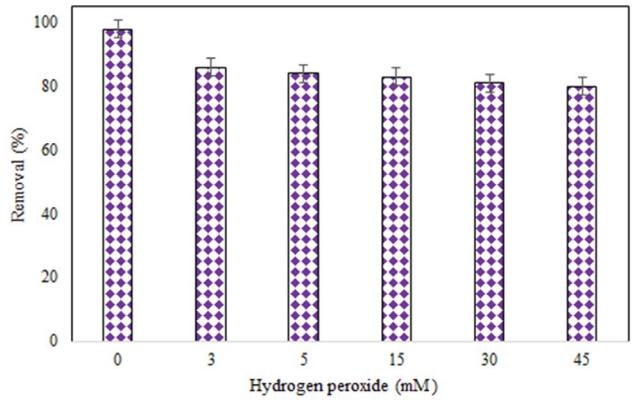

Fig. 7. Influence of H_2O_2 on the photocatalytic degradation of pirimiphos-methyl through silica-functionalized graphene oxide/ZnO.

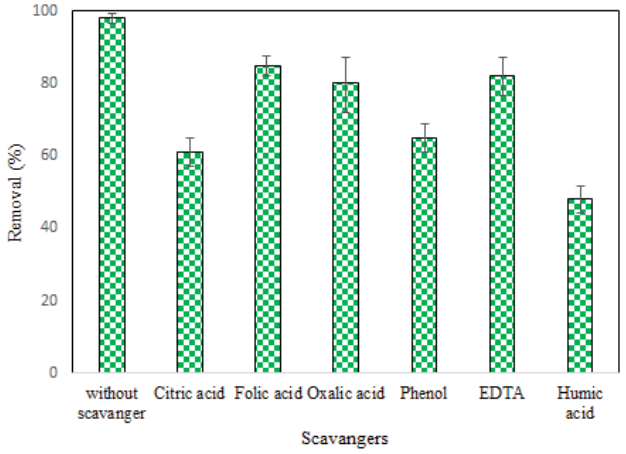

Fig. 8. Influence of different type of organic compounds on the photocatalytic degradation of pirimiphos-methyl through silica-functionalized graphene oxide/ZnO.

excited electrons present in the conduction band of the photocatalyst can produce superoxide radical anion (O_2^-). Another reason for the increased pirimiphos-methyl degradation efficiency in the presence of oxygen can be electron scavenging influence. Dissolved oxygen can effectively react with the electrons generated in the conduction band and prevent the recombination of the positive hole [64]. Therefore, the use of nitrogen as purging gas limits the production of superoxide

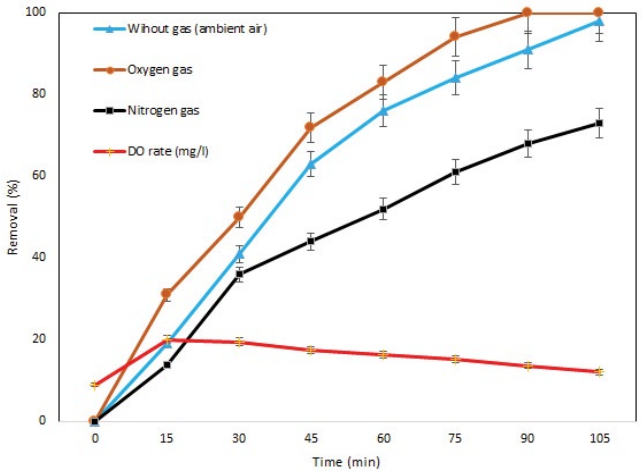

Fig. 9. Influence of effect of different gases purging and variation of DO concentration in photocatalytic degradation of pirimiphos-methyl through silica-functionalized graphene oxide/ZnO.

radicals, creating an environment with less oxidation of pirimiphos-methyl toxin. Another reason for the diminished removal efficiency in the presence of nitrogen is that when the nitrogen gas is bubbled into the reactor, the production of hydroxyl radicals is only due to the degradation of water vapor. Thus, fewer amounts of hydroxyl radicals react with the molecules of the pollutant [54].

3.8. Comparison of each process and reusability

To evaluate the effect of various processes on the photocatalytic degradation of pirimiphos-methyl, the degradation efficiency of pirimiphos-methyl by GO alone, ZnO-alone, GO-ZnO, UV-alone, H_2O_2 alone, UV/H_2O_2, Si-GO-ZnO, and UV/Si-GO-ZnO were compared at the same reaction conditions. The initial concentration of pirimiphos-methyl and the initial pH was 30 mg/L and 7, respectively. Fig. 10 shows that removal efficiency for each process was equal to 40.87%, 5.94%, 24.87%, 25.43%, 26.12%, 46.78%, 27.78%, and 98.00%, respectively. The photocatalytic degradation of pirimiphos-methyl via just adsorption was low. The removal efficiency of pirimiphos-methyl by UV/Si-GO/ZnO process, was greater than other processes. Photocatalytic degradation of pirimiphos-methyl with UV/silica-functionalized graphene oxide-ZnO process was compared with other reported data. This comparison shows that the silica-functionalized graphene oxide/ZnO is an effective catalyst for

the photocatalytic degradation of pirimiphos-methyl from aqueous solution compared to other catalysts and processes.

As the reusability of a photocatalyst after the reaction is an important factor, the photocatalyst loaded with pollutant was placed in the 2 M NaOH solution as a desorbing agent, photocatalytic experiments were repeated five times. As can be seen in Fig. 11, the silica-GO/ZnO showed quite similar photocatalytic activity after 100 min of each photocatalytic reaction during five repeated runs.

3.9. Degradation pathway

The decomposition mechanism of organic compounds with the photocatalytic process is very complicated. In these

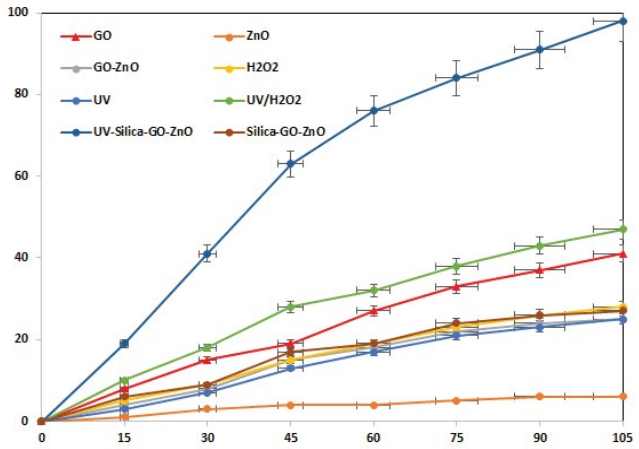

Fig. 10. Contribution of each process involved in the photocatalytic degradation of pirimiphos-methyl.

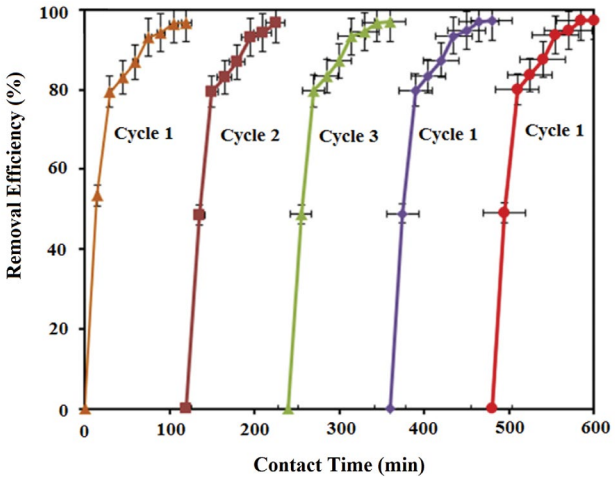

Fig. 11. Reusability test for silica-functionalized graphene oxide/ZnO in photocatalytic degradation of pirimiphos-methyl within five repeated rounds.

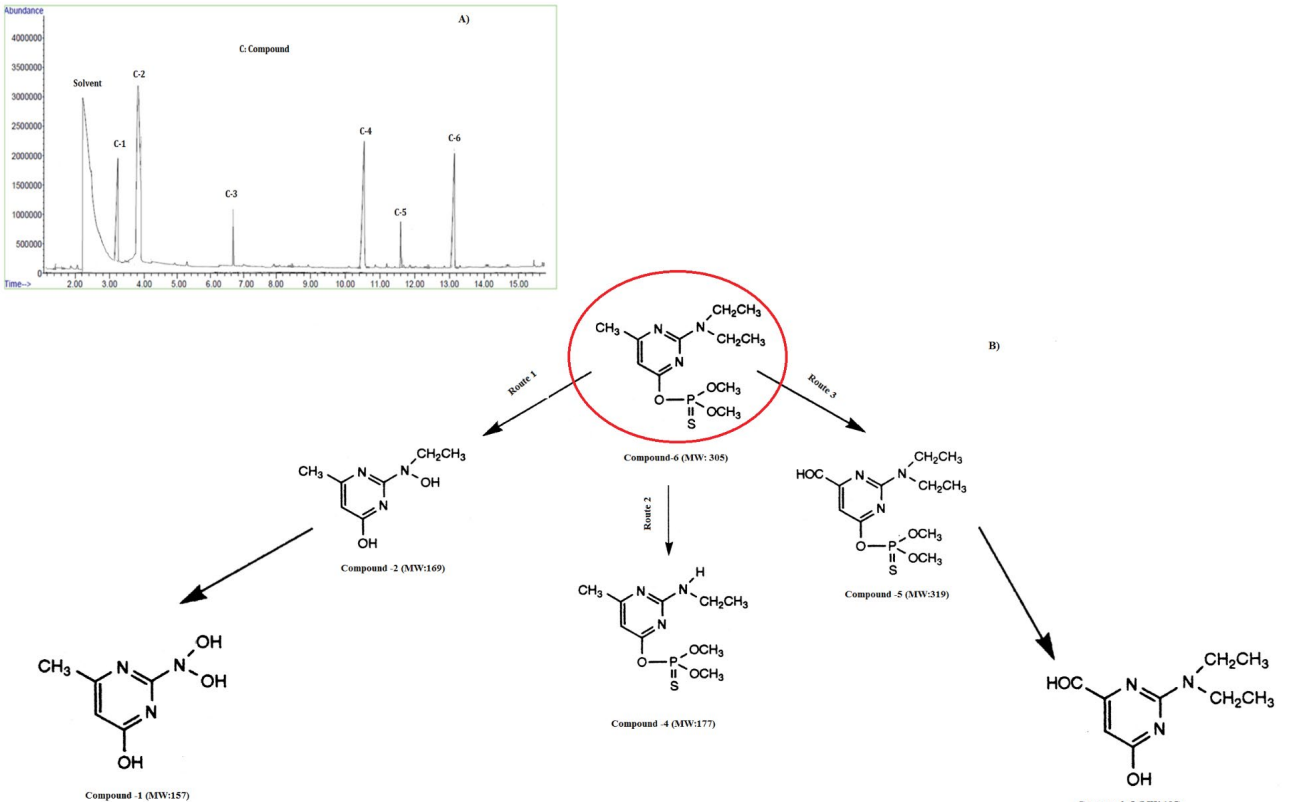

Fig. 12. (a) GC/MS chromatogram of intermediate species of pirimiphos-methyl degradation by the UV/Si-GO-ZnO and (b) possible degradation pathway.

processes, the hydroxyl radical ($OH^{\bullet}$) resulted from the oxidation of adsorbed water or OH^-, is known as the initial oxidizing agent, and the photocatalytic degradation reaction is typically controlled by this radical [65]. The by-products from the decomposition of pirimiphos-methyl in the process exploited in this study (UV/Si-GO/ZnO) are presented in Fig. 12a. According to the by-products observed by GC–MS, the possible route for the decomposition of pirimiphos-methyl by UV/Si-GO/ZnO process is represented in Fig. 12b. As can be seen, there are three major routes of degradation. One route (path 1) may involve the formation of an N-oxime (compound 1) together with the induced hydrolysis of the phosphoric ester function (compound 2). A second path is the result of an N-dealkylation which gives compound 4. A third route involves the oxidation of the methyl group into an aldehyde function (compound 5), followed by the induced hydrolysis of the phosphoric ester function (compound 3). The stability of an aldehyde in an oxidative medium was surprising, but it has been pointed out that aldehydes are oxidized only by radical oxidants, reflecting the slow generation of hydroxy radicals under acidic conditions [66]. However, the proposed mechanism cannot fully explain the degradation of pirimiphos-methyl due to the lack of convincing evidence, and the decomposition path is very complex because of the many small paths, and it is not possible to be expressed certainly.

4. Conclusion

In this study, the photocatalytic degradation of pirimiphos-methyl was investigated using silica-GO/ZnO incorporated fiberglass composite (silica-GO/ZnO). At the optimal conditions of neutral pH (7), initial concentration of pollutant (30 mg/L), and temperature (25°C), and oxygen gas flow (2.5 L/min), 98% of the pollutant was degraded after 100 min contact time. The photocatalytic degradation kinetics of pirimiphos-methyl toxin using the UV-silica-GO/ZnO process had a good fit with the first-order kinetic model. The addition of H_2O_2 resulted in diminished hydroxyl radicals and therefore reduction of the degradation efficiency of the pollutant because of strong scavenging effects. The presence of different organic compounds (folic acid, citric acid, oxalate, phenol, and EDTA) caused the occupation of the active sites present in the catalyst surface and thus, decreased the overall efficiency of the process. The high photocatalytic properties of UV-silica-GO/ZnO will facilitate its application in the environmental photocatalysis field especially for treating water or wastewater containing pirimiphos-methyl.

Acknowledgments

This research work was financially supported by Aja University of medical sciences (AJAUMS) (Grant No. 697722). The authors are grateful for the technical support from the Laboratory of Environmental Health Engineering, Iran University of Medical Sciences.

References

[1] A. Jonidi-Jafari, M. Gholami, M. Farzadkia, A. Esrafili, M. Shirzad-Siboni, Application of Ni-doped ZnO nanorods for degradation of diazinon: kinetics and by-products, Sep. Sci. Technol., 52 (2017) 2395–2406.
[2] S. Yousefzadeh, A.R. Matin, E. Ahmadi, Z. Sabeti, M. Alimohammadi, H. Aslani, R. Nabizadeh, Response surface methodology as a tool for modeling and optimization of *Bacillus subtilis* spores inactivation by UV/nano-Fe^0 process for safe water production, Food Chem. Toxicol., 114 (2018) 334–345.
[3] A.R. Fernandez-Alba, A. Agüera, M. Contreras, G. Peñuela, I. Ferrer, D. Barceló, Comparison of various sample handling and analytical procedures for the monitoring of pesticides and metabolites in ground waters, J. Chromatogr. A, 823 (1998) 35–47.
[4] M.T. Meyer, E.M. Thurman, Herbicide Metabolites in Surface Water and Groundwater, ACS Symposium Series; American Chemical Society, Washington, DC, 1996.
[5] K. Fenner, S. Canonica, L.P. Wackett, M. Elsner, Evaluating pesticide degradation in the environment: blind spots and emerging opportunities, Science, 341 (2013) 752–758.
[6] K. Sharafi, M. Pirsaheb, S. Maleki, H. Arfaeinia, K. Karimyan, M. Moradi, Y. Safari, Knowledge, attitude and practices of farmers about pesticide use, risks, and wastes; a cross-sectional study (Kermanshah, Iran), Sci. Total Environ., 645 (2018) 509–517.
[7] J. Weber, Properties and Behavior of Pesticides in Soil, Mechanisms of Pesticide Movement into Ground Water, CRC Press, Boca Raton, Florida, 2018, pp. 15–42.
[8] C.V. Papazlatani, P.A. Karas, G. Tucat, D.G. Karpouzas, Expanding the use of biobeds: degradation and adsorption of pesticides contained in effluents from seed-coating, bulb disinfestation and fruit-packaging activities, J. Environ. Manage., 248 (2019) 109221.
[9] S.-C. Yang, M. Lei, T.-B. Chen, X.-Y. Li, Q. Liang, C. Ma, Application of zerovalent iron (Fe^0) to enhance degradation of HCHs and DDX in soil from a former organochlorine pesticides manufacturing plant, Chemosphere, 79 (2010) 727–732.
[10] M. Lapertot, S. Ebrahimi, S. Dazio, A. Rubinelli, C. Pulgarin, Photo-Fenton and biological integrated process for degradation of a mixture of pesticides, J. Photochem. Photobiol., A, 186 (2007) 34–40.
[11] P. Chelme-Ayala, M.G. El-Din, D.W. Smith, Kinetics and mechanism of the degradation of two pesticides in aqueous solutions by ozonation, Chemosphere, 78 (2010) 557–562.
[12] P. Frangos, W. Shen, H. Wang, X. Li, G. Yu, S. Deng, J. Huang, B. Wang, Y. Wang, Improvement of the degradation of pesticide deethylatrazine by combining UV photolysis with electrochemical generation of hydrogen peroxide, Chem. Eng. J., 291 (2016) 215–224.
[13] J. Singh, S. Sharma, Aanchal, S. Basu, Synthesis of Fe_2O_3/TiO_2 monoliths for the enhanced degradation of industrial dye and pesticide via photo-Fenton catalysis, J. Photochem. Photobiol., A, 376 (2019) 32–42.
[14] J. Méndez-Díaz, G. Prados-Joya, J. Rivera-Utrilla, R. Leyva-Ramos, M. Sánchez-Polo, M. Ferro-García, N. Medellín-Castillo, Kinetic study of the adsorption of nitroimidazole antibiotics on activated carbons in aqueous phase, J. Colloid Interface Sci., 345 (2010) 481–490.
[15] A. Dargahi, M. Pirsaheb, S. Hazrati, M. Fazlzadehdavil, R. Khamutian, T. Amirian, Evaluating efficiency of H_2O_2 on removal of organic matter from drinking water, Desal. Water Treat., 54 (2015) 1589–1593.
[16] R. Khosravi, M. Fazlzadehdavil, B. Barikbin, H. Hossini, Electro-decolorization of Reactive Red 198 from aqueous solutions using aluminum electrodes systems: modeling and optimization of operating parameters, Desal. Water Treat., 54 (2015) 3152–3160.
[17] R. Khosravi, S. Hazrati, M. Fazlzadeh, Decolorization of AR18 dye solution by electrocoagulation: sludge production and electrode loss in different current densities, Desal. Water Treat., 57 (2016) 14656–14664.
[18] E. Çalişkan, S. Göktürk, Adsorption characteristics of sulfamethoxazole and metronidazole on activated carbon, Sep. Sci. Technol., 45 (2010) 244–255.
[19] R. Khosravi, H. Eslami, A. Zarei, M. Heidari, A.N. Baghani, N. Safavi, A. Mokammel, M. Fazlzadeh, S. Adhami, Comparative

evaluation of nitrate adsorption from aqueous solutions using green and red local montmorillonite adsorbents, Desal. Water Treat., 116 (2018) 119–128.
[20] M. Leili, M. Fazlzadeh, A. Bhatnagar, Green synthesis of nano-zero-valent iron from Nettle and Thyme leaf extracts and their application for the removal of cephalexin antibiotic from aqueous solutions, Environ. Technol., 39 (2018) 1158–1172.
[21] I. Saidi, I. Soutrel, D. Floner, F. Fourcade, N. Bellakhal, A. Amrane, F. Geneste, Indirect electroreduction as pretreatment to enhance biodegradability of metronidazole, J. Hazard. Mater., 278 (2014) 172–179.
[22] A. Almasi, A. Dargahi, A. Amrane, M. Fazlzadeh, M. Mahmoudi, A. Hashemian, Effect of the retention time and the phenol concentration on the stabilization pond efficiency in the treatment of oil refinery wastewater, Fresenius Environ. Bull., 23 (2014) 2541–2548.
[23] M. Farzadkia, E. Bazrafshan, A. Esrafili, J.-K. Yang, M. Shirzad-Siboni, Photocatalytic degradation of Metronidazole with illuminated TiO_2 nanoparticles, J. Environ. Health Sci. Eng., 13 (2015) 35.
[24] E. Azizl, M. Fazlzadeh, M. Ghayebzadeh, L. Hemati, M. Beikmohammadi, H.R. Ghaffari, H.R. Zakeri, K. Sharafi, Application of advanced oxidation process (H_2O_2/UV) for removal of organic materials from pharmaceutical industry effluent, Environ. Prot. Eng., 43 (2017) 183–191.
[25] A. Seid-Mohammadi, A. Shabanloo, M. Fazlzadeh, Y. Poureshgh, Degradation of acid blue 113 by US/H_2O_2/Fe^{2+} and US/$S_2O_8^{2-}$/Fe^{2+} processes from aqueous solutions, Desal. Water Treat., 78 (2017) 273–280.
[26] A.R. Rahmani, A. Shabanloo, M. Fazlzadeh, Y. Poureshgh, H. Rezaeivahidian, Degradation of Acid Blue 113 in aqueous solutions by the electrochemical advanced oxidation in the presence of persulfate, Desal. Water Treat., 59 (2017) 202–209.
[27] J.M. Herrmann, C. Guillard, M. Arguello, A. Agüera, A. Tejedor, L. Piedra, A. Fernández-Alba, Photocatalytic degradation of pesticide pirimiphos-methyl: determination of the reaction pathway and identification of intermediate products by various analytical methods, Catal. Today, 54 (1999) 353–367.
[28] Y. Vasseghian, E.-N. Dragoi, Modeling and optimization of acid blue 193 removal by UV and peroxydisulfate process, J. Environ. Eng., 144 (2018) 06018003–06018007.
[29] D. Son, B.J. Moon, A. Lee, H. Rho, H.J. Lee, T.-W. Kim, J.-S. Ha, S.H. Lee, Polarity effects of ZnO on charge recombination at $CsPbBr_3$ nanoparticles/ZnO interfaces, Appl. Surf. Sci., 483 (2019) 165–169.
[30] M.H. Huang, Y. Wu, H. Feick, N. Tran, E. Weber, P. Yang, Catalytic growth of zinc oxide nanowires by vapor transport, Adv. Mater., 13 (2001) 113–116.
[31] W. Xie, Y. Li, W. Sun, J. Huang, H. Xie, X. Zhao, Surface modification of ZnO with Ag improves its photocatalytic efficiency and photostability, J. Photochem. Photobiol., A, 216 (2010) 149–155.
[32] H. Qin, W. Li, Y. Xia, T. He, Photocatalytic activity of heterostructures based on ZnO and N-doped ZnO, ACS Appl. Mater. Interfaces, 3 (2011) 3152–3156.
[33] G. Wang, X. Yang, F. Qian, J.Z. Zhang, Y. Li, Double-sided CdS and CdSe quantum dot co-sensitized ZnO nanowire arrays for photoelectrochemical hydrogen generation, Nano Lett., 10 (2010) 1088–1092.
[34] D. Chen, D. Wang, Q. Ge, G. Ping, M. Fan, L. Qin, L. Bai, C. Lv, K. Shu, Graphene-wrapped ZnO nanospheres as a photocatalyst for high performance photocatalysis, Thin Solid Films, 574 (2015) 1–9.
[35] K. Woan, G. Pyrgiotakis, W. Sigmund, Photocatalytic carbon-nanotube–TiO_2 composites, Adv. Mater., 21 (2009) 2233–2239.
[36] H. Fu, T. Xu, S. Zhu, Y. Zhu, Photocorrosion inhibition and enhancement of photocatalytic activity for ZnO via hybridization with C60, Environ. Sci. Technol., 42 (2008) 8064–8069.
[37] H. Zhang, X. Lv, Y. Li, Y. Wang, J. Li, P25-graphene composite as a high performance photocatalyst, ACS Nano, 4 (2009) 380–386.
[38] B. Li, T. Liu, Y. Wang, Z. Wang, ZnO/graphene-oxide nano-composite with remarkably enhanced visible-light-driven photocatalytic performance, J. Colloid Interface Sci., 377 (2012) 114–121.
[39] J. Du, X. Lai, N. Yang, J. Zhai, D. Kisailus, F. Su, D. Wang, L. Jiang, Hierarchically ordered macro-mesoporous TiO_2-graphene composite films: improved mass transfer, reduced charge recombination, and their enhanced photocatalytic activities, ACS Nano, 5 (2010) 590–596.
[40] P.-C. Ma, J.-W. Liu, S.-L. Gao, E. Mäder, Development of functional glass fibres with nanocomposite coating: a comparative study, Compos. Part A, 44 (2013) 16–22.
[41] Z. Liu, P. Fang, S. Wang, Y. Gao, F. Chen, F. Zheng, Y. Liu, Y. Dai, Photocatalytic degradation of gaseous benzene with CdS-sensitized TiO_2 film coated on fiberglass cloth, J. Mol. Catal. A: Chem., 363–364 (2012) 159–165.
[42] A.J. Jafari, R.R. Kalantary, A. Esrafili, H. Arfaeinia, Synthesis of silica-functionalized graphene oxide/ZnO coated on fiberglass and its application in photocatalytic removal of gaseous benzene, Proc. Saf. Environ. Prot., 116 (2018) 377–387.
[43] M.V. Lopez-Ramon, F. Stoeckli, C. Moreno-Castilla, F. Carrasco-Marin, On the characterization of acidic and basic surface sites on carbons by various techniques, Carbon, 37 (1999) 1215–1221.
[44] C. Nethravathi, M. Rajamathi, Chemically modified graphene sheets produced by the solvothermal reduction of colloidal dispersions of graphite oxide, Carbon, 46 (2008) 1994–1998.
[45] H. Yan, L. Jiang, X. Xu, Y. Li, Y. Shen, S. Zhu, Ultrastrong composite film of Chitosan and silica-coated graphene oxide sheets, Int. J. Biol. Macromol., 104 (2017) 936–943.
[46] W.L. Zhang, H.J. Choi, Silica-graphene oxide hybrid composite particles and their electroresponsive characteristics, Langmuir, 28 (2012) 7055–7062.
[47] N. Daneshvar, S. Aber, M.S. Seyed Dorraji, A.R. Khataee, M.H. Rasoulifard, Photocatalytic degradation of the insecticide diazinon in the presence of prepared nanocrystalline ZnO powders under irradiation of UV-C light, Sep. Purif. Technol., 58 (2007) 91–98.
[48] A. Ghaly, F. Alkoaik, A. Snow, Degradation of pirimiphos-methyl during thermophilic composting of greenhouse tomato plant residues, Can. Biosyst. Eng., 49 (2007) 6.1–6.11.
[49] Y. Nakaoka, H. Katsumata, S. Kaneco, T. Suzuki, K. Ohta, Photocatalytic degradation of diazinon in aqueous solution by platinized TiO_2, Desal. Water Treat., 13 (2010) 427–436.
[50] M. Shirzad-Siboni, A. Jonidi-Jafari, M. Farzadkia, A. Esrafili, M. Gholami, Enhancement of photocatalytic activity of Cu-doped ZnO nanorods for the degradation of an insecticide: kinetics and reaction pathways, J. Environ. Manage., 186 (2017) 1–11.
[51] S. Yousefzadeh, R. Nabizadeh, A. Mesdaghinia, S. Nasseri, P. Hezarkhani, M. Beikzadeh, M. Valadi Amin, Evaluation of disinfection efficacy of performic acid (PFA) catalyzed by sulfuric and ascorbic acids tested on *Escherichia coli* (ATCC, 8739), Desal. Water Treat., 52 (2014) 3280–3289.
[52] S. Tabasideh, A. Maleki, B. Shahmoradi, E. Ghahremani, G. McKay, Sonophotocatalytic degradation of diazinon in aqueous solution using iron-doped TiO_2 nanoparticles, Sep. Purif. Technol., 189 (2017) 186–192.
[53] X.-J. Wen, C.-G. Niu, L. Zhang, C. Liang, G.-M. Zeng, A novel Ag_2O/CeO_2 heterojunction photocatalysts for photocatalytic degradation of enrofloxacin: possible degradation pathways, mineralization activity and an in depth mechanism insight, Appl. Catal., B, 221 (2018) 701–714.
[54] A.J. Jafari, M. Kermani, R.R. Kalantary, H. Arfaeinia, Photocatalytic abatement of *o*-xylene using adsorption enhanced ZnO/GAC catalyst in a continuous flow reactor: catalytic potential, Global Nest J., 19 (2017) 479–488.
[55] R.R. Kalantary, Y. Dadban Shahamat, M. Farzadkia, A. Esrafili, H. Asgharnia, Photocatalytic degradation and mineralization of diazinon in aqueous solution using nano-TiO_2 (Degussa, P25): kinetic and statistical analysis, Desal. Water Treat., 55 (2015) 555–563.
[56] B. Shahmoradi, M. Negahdary, A. Maleki, Photodegradation of methylene blue using surface modified manganese doped TiO_2 nanoparticles, Environ. Eng. Sci., 29 (2012) 1032–1037.

[57] H. Arfaeinia, B. Ramavandi, K. Sharafi, S. Hashemi, Reductive degradation of ciprofloxacin in aqueous using nanoscale zero valent iron modificated by Mg-aminoclay, Int. J. Pharm. Technol., 8 (2016) 13125–13136.
[58] A. Stasinakis, Use of selected advanced oxidation processes (AOPs) for wastewater treatment–a mini review, Global Nest J., 10 (2008) 376–385.
[59] H.B. Senturk, D. Ozdes, A. Gundogdu, C. Duran, M. Soylak, Removal of phenol from aqueous solutions by adsorption onto organomodified Tirebolu bentonite: equilibrium, kinetic and thermodynamic study, J. Hazard. Mater., 172 (2009) 353–362.
[60] C.-K. Wang, Y.-H. Shih, Facilitated ultrasonic irradiation in the degradation of diazinon insecticide, Sustainable Environ. Res., 26 (2016) 110–116.
[61] Y.-S. Ma, Short review: current trends and future challenges in the application of sono-Fenton oxidation for wastewater treatment, Sustainable Environ. Res., 22 (2012) 271–278.
[62] N. Wang, L. Zhu, M. Wang, D. Wang, H. Tang, Sono-enhanced degradation of dye pollutants with the use of H_2O_2 activated by Fe_3O_4 magnetic nanoparticles as peroxidase mimetic, Ultrason. Sonochem., 17 (2010) 78–83.
[63] X. Van Doorslaer, P.M. Heynderickx, K. Demeestere, K. Debevere, H. Van Langenhove, J. Dewulf, TiO_2 mediated heterogeneous photocatalytic degradation of moxifloxacin: operational variables and scavenger study, Appl. Catal., B, 111 (2012) 150–156.
[64] A. Jonidi-Jafari, M. Shirzad-Siboni, J.-K. Yang, M. Naimi-Joubani, M. Farrokhi, Photocatalytic degradation of diazinon with illuminated ZnO–TiO_2 composite, J. Taiwan Inst. Chem. Eng., 50 (2015) 100–107.
[65] K.-P. Yu, G.W.M. Lee, Decomposition of gas-phase toluene by the combination of ozone and photocatalytic oxidation process (TiO_2/UV, TiO_2/UV/O_3, and UV/O_3), Appl. Catal., B, 75 (2007) 29–38.
[66] C. Crescenzi, A. Di Corcia, E. Guerriero, R. Samperi, Development of a multiresidue method for analyzing pesticide traces in water based on solid-phase extraction and electrospray liquid chromatography mass spectrometry, Environ. Sci. Technol., 31 (1997) 479–488.